Proc. Natl. Acad. Sci. USA
Vol. 93, pp. 1021–1026, February 1996
Biophysics

Structural changes of tumor necrosis factor α associated with membrane insertion and channel formation

(cytokine/conformation/photolabeling/molten globule/pH dependency)

RAE LYNN BALDWIN*†, MARK L. STOLOWITZ‡, LEROY HOOD‡, AND BERNADINE J. WISNIESKI*§

*Department of Microbiology and Molecular Genetics, the Molecular Biology Institute, and the Jonsson Comprehensive Cancer Center, University of California, Los Angeles, CA 90095; and ‡Department of Molecular Biotechnology, Mailstop FJ-20, University of Washington, Seattle, WA 98195

Contributed by Leroy Hood, September 5, 1995

ABSTRACT **Low pH enhances tumor necrosis factor α (TNF)-induced cytolysis of cancer cells and TNF–membrane interactions that include binding, insertion, and ion-channel formation. We have also found that TNF increases Na^+ influx in cells. Here, we examined the structural features of the TNF–membrane interaction pathway that lead to channel formation. Fluorometric studies link TNF's acid-enhanced membrane interactions to rapid but reversible acquisition of hydrophobic surface properties. Intramembranous photolabeling shows that (*i*) protonation of TNF promotes membrane insertion, (*ii*) the physical state of the target bilayer affects the kinetics and efficiency of TNF insertion, and (*iii*) binding and insertion of TNF are two distinct events. Acidification relaxes the trimeric structure of soluble TNF so that the cryptic carboxyl termini, centrally located at the base of the trimer cone, become susceptible to carboxypeptidase Y. After membrane insertion, TNF exhibits a trimeric configuration in which the carboxyl termini are no longer exposed; however, the proximal salt-bridged Lys-11 residues as well as regional surface amino acids (Glu-23, Arg-32, and Arg-44) are notably more accessible to proteases. The sequenced cleavage products bear the membrane-restricted photoreactive probe, proof that surface-cleaved TNF has an intramembranous disposition. In summary, the trimer's structural plasticity is a major determinant of its channel-forming ability. Channel formation occurs when cracked or partially splayed trimers bind and penetrate the bilayer. Reannealing leads to a slightly relaxed trimeric structure. The directionality of bilayer penetration conforms with x-ray data showing that receptor binding to the monomer interfaces of TNF poises the tip of the trimeric cone directly above the target cell membrane.**

The soluble active form of tumor necrosis factor α (TNF, or cachectin) is a 52-kDa trimer, which is secreted primarily by activated macrophages (1). Exploitation of TNF's potent antitumor activities and other beneficial roles has been hampered by the fact that high local and systemic levels of TNF provoke a host of debilitating and often lethal sequelae (2, 3). How this cytokine induces such a wide variety of responses is not well understood. Only two types of TNF receptors have been identified (4–6), and the majority of cells in the body bear one or both (7). Thus, receptor presence in itself is not sufficient to account for the diversity of cell-type-specific responses. There are also reports of receptor-independent responses (8–12). Consequently, variations in TNF–cell interactions and postreceptor pathways must account for the myriad of potential effects.

It remains controversial whether receptor-mediated endocytosis is obligatory for TNF's biological activity (7, 13, 14). In some cell types, functional lysosomes and cytoskeletal integrity appear necessary for TNF-dependent cytotoxicity (15, 16), and lysosomal function is impaired as TNF resistance develops (17). When liposome-encapsulated TNF was antibody-targeted to cells that lacked receptors, cytostasis was induced (12). The protocol for attaching antibodies involved exposing the encapsulated TNF to slightly acidic pH. We have shown that extracellular acidification of TNF (pH 5.3, 15 min) markedly enhances its cytolytic activity toward human U937 histiocytic leukemia cells (18, 19). Lysosomotropic agents had a very slight enhancing effect on TNF's killing activity at neutral pH, and in conjunction with extracellular acidification led to an increase in cell killing far beyond that seen with acidification alone (19). We speculated that low pH facilitates TNF insertion into the plasma membrane and that lysosomotropic agents inhibit the degradation of an endocytosed pool of TNF. The same low pH treatment that leads to enhanced cell killing (18, 19) diminishes specific receptor binding and increases both nonspecific and total binding. It also enhances TNF-dependent inhibition of adipocyte differentiation, a model for TNF's cachectic activity (unpublished data). Thus, acidification of TNF [e.g., at macrophage–target cell junctions (20) or in acidic organelles] may have a physiologically significant role. By analogy with influenza virus and diphtheria toxin (21), it may favor a structural state required for membrane penetration. The β-jellyroll motif of TNF resembles the coat protein structures of several viruses (22, 23), and a direct comparison of the cytotoxic processes of TNF and diphtheria toxin has revealed a number of striking similarities (19).

In our quest to unravel TNF structure–function relationships, we discovered that TNF increases intracellular Na^+ and forms ion channels in planar bilayer targets (24). Low pH promotes TNF insertion into the bilayer (i.e., channel formation *per se*); transmembrane voltage regulates channel opening (25). The structurally and functionally related TNF-β (lymphotoxin) expresses similar activity (25–27). Depending on local conditions, TNF channel formation could lead to subtle changes in ion conductance or substantial membrane depolarization, changes commensurate with physiological observations (reviewed in refs. 24 and 26), including the drop in membrane resting potential of skeletal muscle cells and fluid accumulation in hypotensive shock.

Because the acid-enhanced activities of TNF noted with target cells and artificial membranes are likely to be related, we aimed to understand the structure of membrane-embedded TNF and the constraints on membrane binding and insertion. It appears that low pH induces reversible conformational changes that strongly favor interactions with membrane lipids. These changes, including cracking of intersheet contacts, are

The publication costs of this article were defrayed in part by page charge payment. This article must therefore be hereby marked "*advertisement*" in accordance with 18 U.S.C. §1734 solely to indicate this fact.

Abbreviations: TNF, tumor necrosis factor α; ANS, 8-anilino-1-naphthalenesulfonic acid; 12APS-GlcN, 12-(4-azido-2-nitrophenoxy) stearoyl[1-^{14}C]glucosamine; DMPC, dimyristoyl phosphatidylcholine.

†Present address: Department of Ob/Gyn, Cedars-Sinai Medical Center, 8700 Beverly Boulevard, Los Angeles, CA 90048.
§To whom reprint requests should be addressed at: Department of Microbiology and Molecular Genetics, 1602 Molecular Sciences Building, University of California, Los Angeles, CA 90095.

largely reversed after membrane penetration. The externally exposed surface of the membrane-embedded trimer is distinctive in that specific sites are either uniquely resistant or exquisitely sensitive to proteolytic attack. Thus, TNF membrane penetration involves a partially disordered molten globule-like transition state (28) that subsequently acquires a more ordered though not completely native conformation.

MATERIALS AND METHODS

Materials. Studies conducted with human recombinant TNF (2.5 mg/ml) from Smith Kline & French were subsequently repeated with clinical-grade human recombinant TNF (0.5 mg/ml) from Genentech. The photoreactive glycolipid probe 12-(4-azido-2-nitrophenoxy)stearoyl[1-^{14}C]glucosamine (12APS-GlcN; 50–60 μCi/μmol) was synthesized as described (29). 8-Anilino-1-naphthalenesulfonic acid (ANS) was from Eastman Kodak, and dimyristoyl phosphatidylcholine (DMPC) was from Avanti. SCP buffer is a 0.15 M sodium citrate/phosphate/chloride constant-ionic-strength buffer made from 1 M stocks as described (27).

Vesicle Binding and Intramembranous Photolabeling. Briefly, unilamellar DMPC vesicles (≈500-Å diameter) prepared in SCP buffer at defined pH values were mixed with 12APS-GlcN (40,000 cpm/50 μg of DMPC/200 μl of SCP buffer). After incubation with TNF, vesicles were irradiated at 366 nm for 1 min, purified by flotation through Ficoll 400 step gradients at pH 8 and subjected to SDS/PAGE (12.5% gels; reduced) and fluorography. See ref. 27 for details.

Crosslinking. ^{125}I-labeled TNF (0.1 μg; 5.68 × 10^6 cpm/μg) prepared by the Iodo-Gen method (Pierce) was mixed with

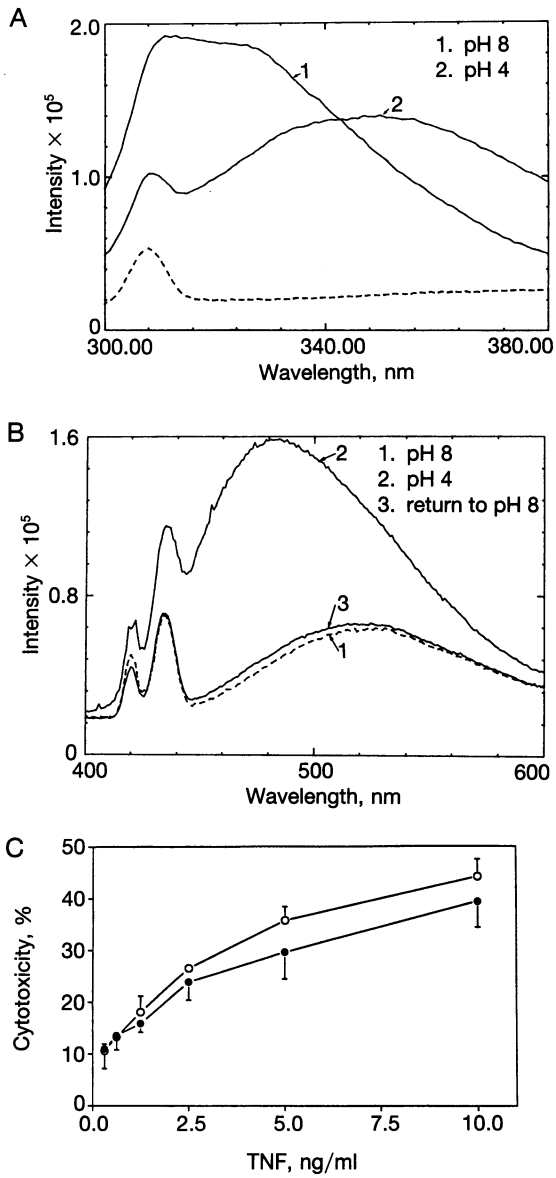

FIG. 1. Effects of low pH on TNF. (*A*) Intrinsic fluorescence of TNF (10 μg) at 37°C in 2 ml of SCP buffer at pH 8 (scan 1) and pH 4 (scan 2). The spectrum of pH 8 buffer is the dashed line. Emission spectra are the sum of 5 scans with excitation at 280 nm (27). (*B*) ANS interactions with TNF. TNF (10 μg) was incubated with 4 μM ANS in SCP buffer. The pH was shifted from pH 8 (scan 1) to pH 4 (scan 2) by addition of 1 M HCl. After 20 min, the pH was returned to pH 8 (scan 3) by addition of 1 M NaOH. Scan of ANS in the absence of TNF is identical to scan 1. Scans were summed as above; excitation was at 380 nm. (*C*) ^{51}Cr-loaded U937 cells (1 × 10^4 in 200 μl of RPMI 1640 medium + 5% calf serum) were incubated with untreated TNF (○) or TNF that was preincubated at pH 4 for 15 min at 37°C (●). After cells were incubated for 20 hr at 37°C, cytolysis was quantified as described (18, 19).

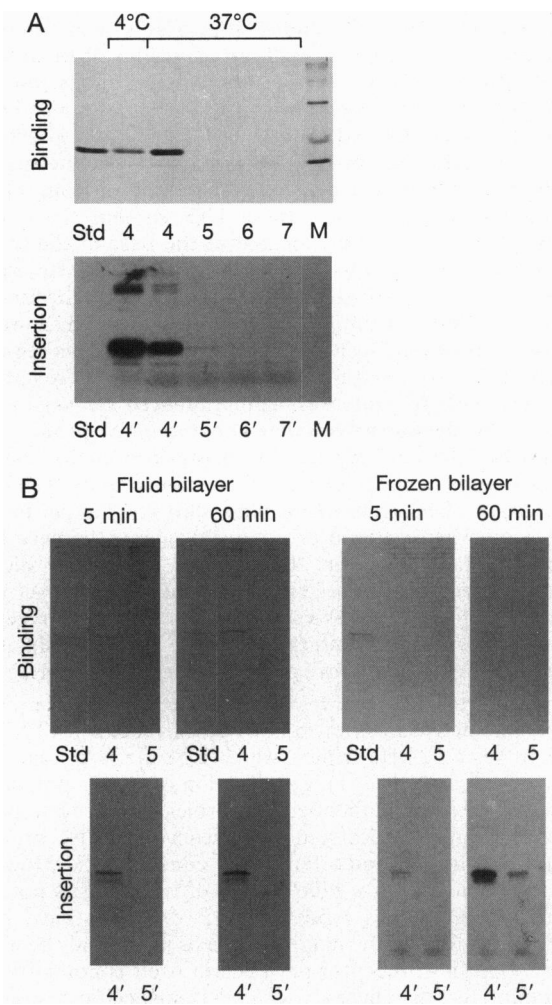

FIG. 2. Factors affecting TNF membrane binding and insertion. (*A*) Dependency on pH. TNF (7.5 μg) was incubated with 12APS-GlcN-containing DMPC vesicles (50 μg) at the designated temperatures (at top of lanes) and pH values (at bottom of lanes) prior to irradiation. (*A Upper*) Vesicle-bound TNF assessed by Coomassie blue staining. (*A Lower*) Bilayer-inserted (photolabeled) TNF detected by fluorography. Lanes: Std, 3 μg of TNF standard; 4–7 (4′–7′), pH values; M, molecular mass: standards defined in Fig. 4*A*. (*B*) Dependency on time and membrane physical state. 12APS-GlcN-containing vesicles and TNF were incubated as indicated prior to irradiation. (*B Upper*) Vesicle-bound TNF (Coomassie blue-stained gels). (*B Lower*) Vesicle-embedded TNF (corresponding fluorograms). Lanes: Std, 4 μg of TNF standard; 4 and 5 (4′ and 5′), pH values.

0.71 μg of unlabeled TNF prior to incubation with 50 μg of DMPC vesicles in 50 μl of pH 4 SCP buffer for 1 hr at 37°C or 4°C. A protein-to-lipid ratio 1/10th of normal was employed to favor detection of dissociated TNF trimers. Vesicles were purified by flotation and brought to 40 μl with pH 8 SCP buffer. Soluble TNF (0.05 μg labeled + 0.35 μg unlabeled; amount equivalent to vesicle-bound) was suspended in 40 μl of pH 8 SCP buffer. Glutaraldehyde treatment (1 μl of 4% stock) was for 15 min. Samples were then mixed with 20 μl of 2×-reducing buffer, boiled, and subjected to SDS/PAGE (12.5% gels) and autoradiographic analysis.

Proteolysis of Soluble and Membrane-Associated TNF. TNF (2 μg in 4 μl of phosphate-buffered saline, pH 7.4 at 37°C) was added to 12.5 μg of fluid-phase DMPC vesicles in 11 μl of pH 4 SCP buffer at 37°C. After 15 min at 37°C, two volumes of pH 8 SCP buffer was added (except for samples cleaved with carboxypeptidase Y at low pH, which received 2 volumes of pH 4 SCP buffer). Acid-pulsed soluble TNF was prepared in the absence of vesicles. Control soluble TNF was prepared by adding premixed pH 4/pH 8 SCP buffer, 1:2 (vol/vol), prior to cleavage. Samples were incubated at 37°C for 2 hr with 1 μg of endoproteinase Lys-C (Boehringer Mannheim), carboxypeptidase Y (Sigma), or V8 protease (Sigma) added in 10 μl of buffer. Vesicle-bound TNF was purified by flotation. With endoproteinase Arg-C (Pierce), ≈2 μg of vesicle-bound TNF was separated from unbound TNF before cleavage with 0.15 μg of Arg-C at 37°C for 12 hr. For amino acid sequencing, samples contained 10–15 μg of TNF and were scaled up accordingly. Unless indicated, cleaved samples were run reduced on tricine/SDS/polyacrylamide gels (16.5% T/6% C separating; 10% T/3% C spacer; 4% T/3% C stack [30]), which were analyzed by fluorography. Bands on protein-stained Immobilon P (Millipore) blots (31) were identified with an Applied Biosystems Protein Sequencer (model 477).

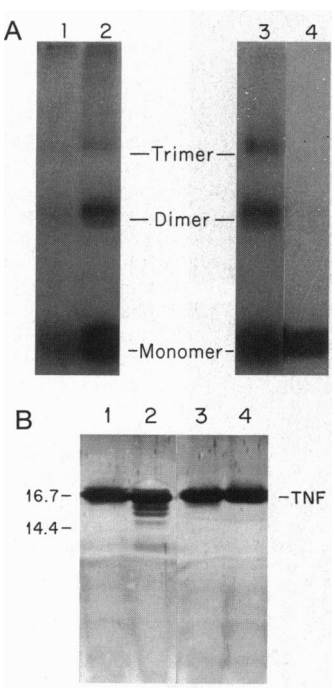

FIG. 3. The quaternary structure of vesicle-bound TNF. (*A*) Vesicle-bound and soluble ^{125}I-labeled TNF were chemically crosslinked at pH 8. Autoradiogram lanes: 1, TNF bound to frozen DMPC vesicles (4°C) at pH 4 for 60 min; 2, TNF bound to fluid DMPC vesicles (37°C) at pH 4 for 60 min; 3, soluble TNF; 4, soluble TNF that was not crosslinked. (*B*) The carboxyl terminus of soluble TNF is exposed at low pH. Silver-stained gel lanes: 1, control TNF cleaved with carboxypeptidase Y at pH 8; 2, TNF cleaved at pH 4; 3, membrane-inserted TNF cleaved at pH 8; 4, acid-pulsed TNF cleaved at pH 8.

RESULTS

Intrinsic Fluorescence of TNF as a Function of pH. The intrinsic fluorescence of soluble TNF decreased dramatically when the pH was lowered from 8 to 4 (Fig. 1*A*), indicating that the tryptophan residues of TNF shifted from a hydrophobic to a polar environment (24, 27). The maximum emission wavelength (λ_{max}) at pH 8 was 328 nm, whereas that at pH 4 was 350 nm. This red shift is likewise typical of a shift of tryptophan to a polar environment (24, 27), which could result in protein acquisition of hydrophobic surface properties. When the pH was returned to 8 (data not shown), the λ_{max} decreased rapidly to 328 nm. The peak at 308 nm reflects the Raman scatter of water.

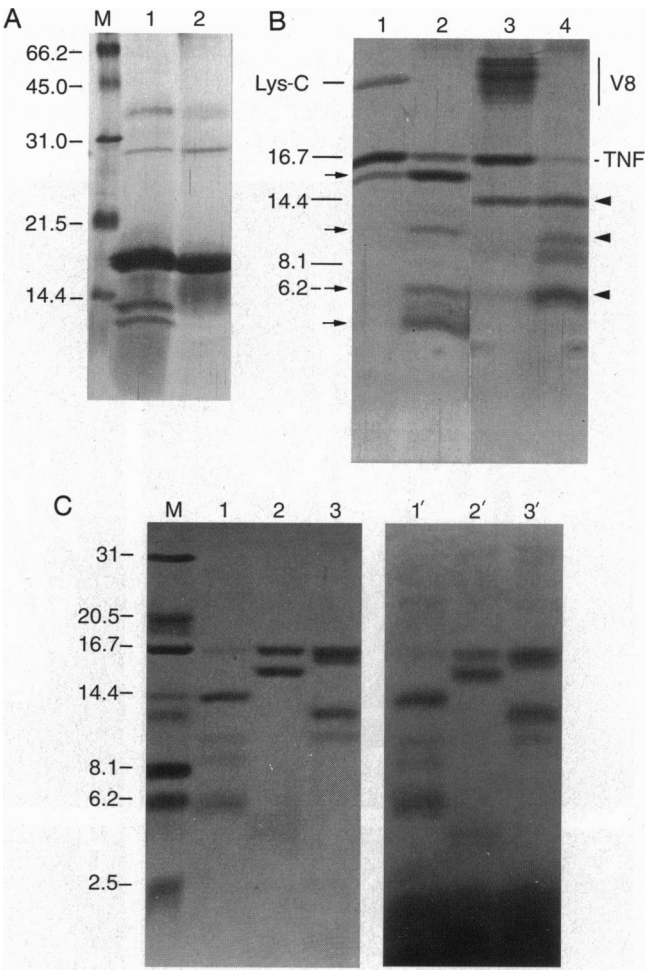

FIG. 4. Proteolysis of vesicle-bound TNF and soluble TNF. (*A*) Endoproteinase Arg-C cleavage. Samples were cleaved with endoproteinase Arg-C (0.025 units; 0.15 μg) as described; SDS-PAGE was on a 19% polyacrylamide gel. Lanes: M, molecular mass standards in kDa; 1, vesicle-embedded TNF; 2, soluble TNF. (*B*) Samples were cleaved with 1 μg of endoproteinase Lys-C or V8 protease for 2 hr at 37°C as described. A silver-stained gel is shown. Lanes: 1, soluble TNF cleaved with Lys-C; 2, membrane-inserted TNF cleaved with Lys-C; 3, soluble TNF cleaved with V8 protease; 4, vesicle-embedded TNF cleaved with V8 protease. Protease and molecular mass marker positions are indicated. Bands marked with an arrow contain an amino-terminal sequence beginning with Pro-12 (lanes 1 and 2); bands marked with an arrowhead begin with Gly-24 (lanes 3 and 4). (*C*) Vesicle-embedded TNF was photolabeled from within the hydrophobic core of the lipid bilayer as described. Coomassie blue-stained gel (lanes 1–3) and fluorogram (lanes 1′–3′) show V8 protease-cleaved samples (lanes 1 and 1′), endoproteinase LysC-cleaved samples (lanes 2 and 2′), and endoproteinase ArgC-cleaved samples (lanes 3 and 3′). Molecular mass markers (lane M) are shown in kDa.

The Interaction of ANS with TNF. Lowering the pH of a solution of TNF and ANS caused a dramatic increase in ANS fluorescence and a blue shift in its λ_{max} from 525 nm to 485 nm (Fig. 1*B*). These spectral changes demonstrate that TNF acquires hydrophobic binding sites for ANS at low pH (27, 32). Shifting the pH from 4 back to 8 resulted in a return to the original pH 8 spectrum, indicating complete loss of hydrophobic binding sites on TNF. Indeed, preexposure of TNF to pH 4 had little effect on biological activity (Fig. 1*C*). At pH 8, the fluorescence spectra of ANS in the absence and presence of TNF are superimposable; hence, TNF lacks hydrophobic binding sites for ANS at pH 8. Shifting the pH between 8 and 4 in the absence of TNF had no effect on the ANS spectrum.

Membrane Binding and Insertion Activities of TNF. TNF binding to pure DMPC vesicles (melting temperature t_m = 23°C) decreased with increasing pH (Fig. 2*A Upper*). Although less TNF bound to frozen vesicles (4°C) than to fluid vesicles (37°C) at pH 4 (Fig. 2*A Upper*), photolabeling with the intramembranous probe 12APS-GlcN (33) revealed that a significantly larger proportion of it inserted into the hydrocarbon core of the bilayer (Fig. 2*A Lower*).

After incubation for 5 and 60 min, the extents of TNF binding to fluid DMPC vesicles (37°C) at pH 4 were 35% and 65% (Fig. 2*B Upper*). At pH 5, TNF binding to fluid vesicles was barely detectable, even after 60 min. In this study, no binding was detectable at higher pH. TNF binding to frozen vesicles (4°C) was not apparent until 60 min, when a low level of binding was observed. No binding was detected at pH 5.

Photolabeling data in Fig. 2*B* (*Lower*) demonstrate that a significant level of TNF insertion had occurred after the 5-min incubation at pH 4 with fluid vesicles and that incubation for 60 min led to a slightly higher level of insertion. At pH 5, clear detection of TNF insertion required a 60-min incubation, although a very faint level was seen at 5 min. With frozen vesicles, the level of insertion increased more notably with incubation time and was similarly higher at pH 4 than at pH 5 (Fig. 2*B Lower*). Despite the lower binding efficiency with frozen vesicles, the levels of inserted TNF observed at both pH values and at both times were significantly higher with frozen vesicles than with fluid vesicles.

The Quaternary Structure of Membrane-Associated TNF. Chemical crosslinking analysis of the oligomeric nature of

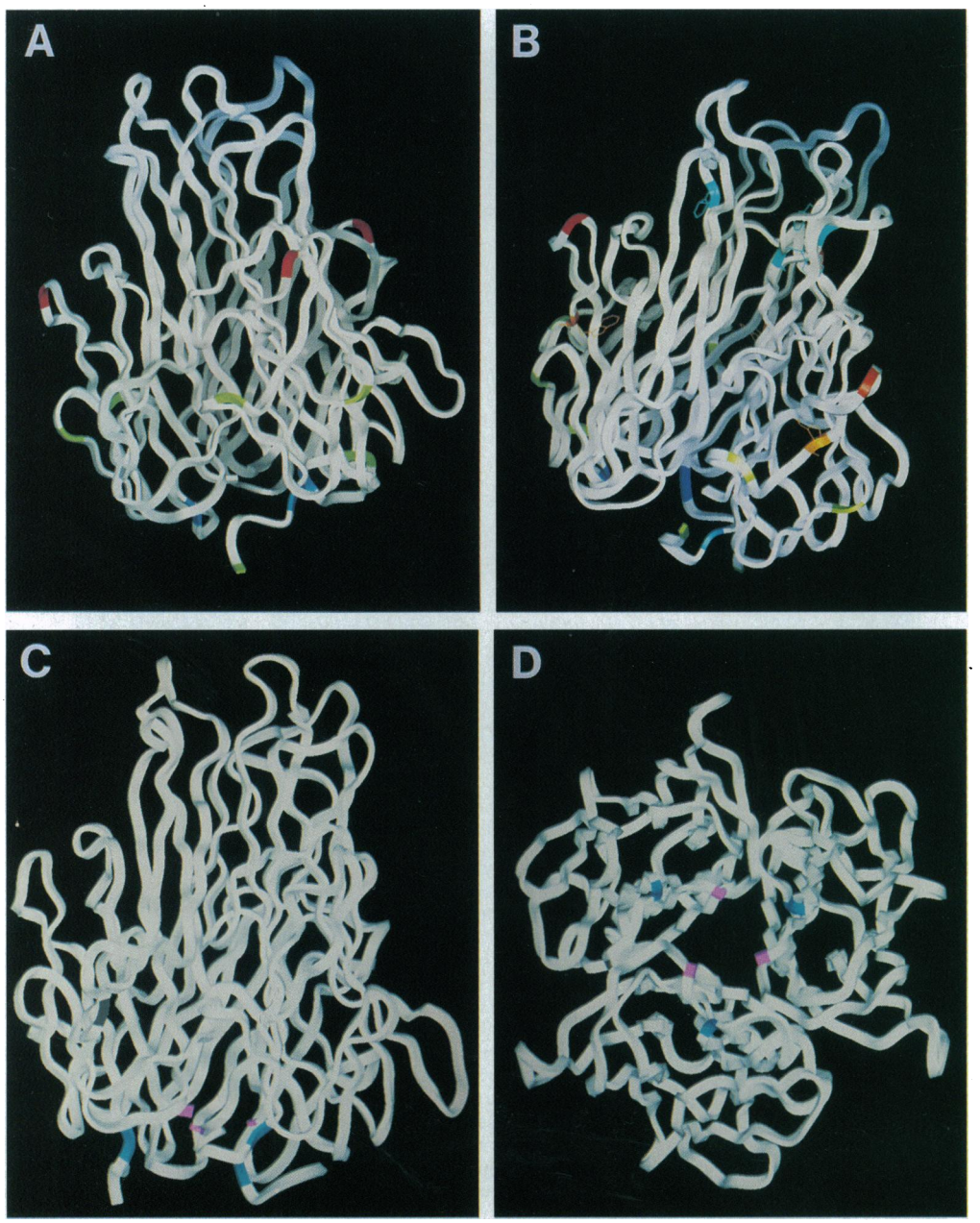

FIG. 5. Sites of detected changes in TNF conformation. (*A*) Residues that become more accessible to endoproteinase Arg-C and protease V8 when TNF is membrane-inserted. Right front subunit: Arg-6 (bottom-most green residue, first definable residue in the x-ray structure), Arg-32 (above Arg-6, green), Arg-44 (directly to the right of arg-32, green); Glu-23 (red). (*B*) Residues depicted in *A* plus Trp-28 (orange) and Trp-114 (turquoise), residues that shift to a polar environment when soluble TNF is acidified. (*C* and *D*) The Lys-11 (blue) to Leu-157 (pink) ion pairs. After TNF membrane insertion, Lys-11 is accessible to endoproteinase Lys-C, and Leu-157 is inaccessible to carboxypeptidase Y, regardless of assay pH. Leu-157 of soluble TNF is only accessible to carboxypeptidase Y at low pH. (*D*) Bottom view of the central "pore-like region" of TNF, which may be involved in voltage-gated channel activity. The x-ray coordinates of TNF are those of Eck and Sprang (23); imaging software is INSIGHT II, version 2.3.0 (Biosym Technologies).

vesicle-associated TNF revealed that regardless of whether TNF was bound to fluid or frozen DMPC vesicles, it exhibited the same crosslinking profile as native TNF in solution (Fig. 3*A*). Indeed, equivalent proportions of TNF trimers, dimers, and monomers were detected in crosslinked samples of frozen membrane-associated TNF (Fig. 3*A*, lane 1), fluid membrane-associated TNF (Fig. 3*A*, lane 2) and soluble native TNF (Fig. 3*A*, lane 3). Additional studies showed that acid-pulsed soluble TNF yielded the same profile as native TNF. Thus, all of the low pH-induced conformational changes observed reflect reorganizations compatible with retention or rapid reacquisition of a trimer-like structure.

Susceptibility of Vesicle-Bound TNF to Proteolysis. To determine whether the structure of membrane-embedded TNF differs from the structures of native and acid-treated soluble TNF, we analyzed the susceptibilities of these forms to enzymic digestion (Fig. 3*B*). At neutral pH, native TNF, acid-pulsed TNF, and membrane-embedded TNF all exhibited structures in which β-strand h (carboxyl-terminal) and contiguous residues were buried. At low pH, the carboxyl termini of soluble TNF became accessible to cleavage by carboxypeptidase Y (Fig. 3*B*, lane 2). In contrast, the carboxyl termini of membrane-embedded TNF remained inaccessible at pH 4. Thus, membrane penetration locks this region into a pH-independent conformation.

At pH 8, endoproteinase Arg-C-mediated cleavage of soluble TNF generates a 16.6-kDa fragment (Fig. 4*A*). This fragment and uncleaved TNF appear as a doublet. Identical results were obtained with acid-pulsed soluble TNF (data not shown). In contrast, vesicle-bound TNF was more sensitive to Arg-C cleavage. Fragment masses and sequence analysis of the three major products indicate that 16.6 kDa consists of amino acid residues 7–157, that 13.5 kDa consists of residues 33–157, and that 12.4 kDa consists of residues 45–157. Thus, membrane insertion leads to increased cleavage at Arg-6, Arg-32, and Arg-44.

Studies with endopeptidase Lys-C and V8 protease (Fig. 4*B*) revealed that residues Lys-11 and Glu-23 are also more accessible in the membrane-embedded form of TNF. The fact that fragments bear the membrane-restricted photoreactive probe (Fig. 4*C*) proves that the surface cleavage sites reside on the membrane-inserted form of TNF. The data gathered thus far demonstrate that the membrane-embedded form of the TNF is a trimer that is not strictly identical to the soluble native form or the soluble acid-pulsed form.

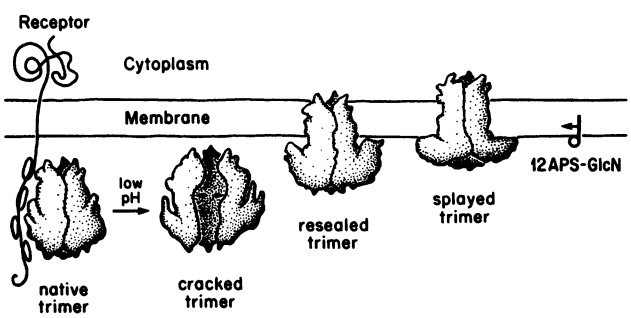

FIG. 6. The membrane insertion pathway of TNF. Receptor binding (only one receptor is shown) poises the TNF trimer directly above the membrane (36). Low pH promotes surface exposure of hydrophobic residues (e.g., Leu-157, Trp-28, and Trp-114). Trimer cracking is indicated by Leu-157 exposure. After TNF penetrates the membrane via the top portion of the cone-like structure, intersubunit cracks are repaired. Synthetic peptides that mimic the topmost loop of TNF have trypanolytic activity (10). Enhanced exposure of Lys-11, Arg-32, and Arg-44 indicates that the surface region containing the shorter β-strands and connecting loops has acquired a relaxed conformation. Two levels of unfurling are shown. A larger hydrophobic surface is uncovered in the structure on the right, allowing TNF to sink deeper into the bilayer. The arrow on the glycolipid probe 12APS-GlcN represents the photoreactive arylazido group.

DISCUSSION

The results of this investigation increase our understanding of the structures of the insertion-competent and membrane-embedded forms of TNF. As shown in Fig. 5, TNF exists as a compact conical-shaped trimer ≈60 Å long and 40 Å wide at the base (22, 23). The outer surface is predominantly polar, and intersubunit edge-to-face contacts bury a large number of amphipathic residues. A long "pore-like region" spans the central axis (23).

Exposure of tryptophan residues to a hydrophilic milieu at low pH is consistent with increased surface hydrophobicity. Trp-114 (Fig. 5*B*, turquoise) resides within β-strand f (residues 112–125), the longest internal peptide chain (see ref. 34 for β-strand designation). It is the first ordered residue after the poorly ordered e–f loop region at the topmost portion of the trimer cone (34). While Trp-114 is buried at pH 7.4 (34, 35), protonation of nearby residues (e.g., Glu-116, a salt-bridge participant) could readily expose it to an aqueous milieu. Trp-28 (Fig. 5*B*, orange) is located in β-strand a′ (residues 26–30). Although this strand and the following loop (residues 31–35) are surface structures, Trp-28 faces inward at pH 7.4 (34, 35). Interestingly, Trp-28 resides in the region of loose secondary structure that contains residues shown to become highly accessible to proteases Arg-C and V8 after TNF membrane insertion—i.e., Glu-23 (red), Arg-32 (green), and Arg-44 (green) (Fig. 5 *A* and *B*). Neutralization of acid-treated soluble TNF returns this looping surface structure to a native-like conformation, as demonstrated by the blue-shift of tryptophan fluorescence and resistance to proteases Arg-C and V8. In contrast, neutralization of membrane-inserted TNF has no detectable effect on the acid-induced conformation of this region; its exquisite sensitivity to proteases Arg-C and V8 remains uniquely independent of assay pH. Therefore, membrane penetration stabilizes the looser "acid configuration" of this particular region. Proof that the surface-exposed cleavage sites belong to membrane-embedded TNF (Fig. 6) is that proteolysis of photolabeled vesicle-bound TNF generated 12APS-GlcN-bearing peptides (Fig. 4*C*).

In the case of soluble TNF, rapid reversibility of acid-induced structural changes is reflected in loss of ANS binding (Fig. 1*B*), loss of affinity for lipid vesicles (the 5-min and 60-min samples in Fig. 2*B* would not be different if raising the pH did not stop binding and insertion), and normal levels of biological activity (Fig. 1*C*). TNF's acquisition of ANS binding sites under acidic conditions is just one of several characteristics that suggests attainment of a partially disordered molten globule-like state, a relatively stable intermediate in the protein-folding pathway that appears to be necessary for membrane penetration (28).

The TNF trimer contains four salt-bridges—i.e., Lys-98 to Glu-116, Lys-11 to the α-carboxylate of Leu-157, Arg-32 to Glu-146, and Arg-103 to Glu-104 (23, 34, 35). The Lys-11–Leu-157 ion pair (Fig. 5 *C* and *D*, blue–pink) stabilizes monomer–monomer contacts that encircle the internal "pore-like region" of TNF (23). Acid-induced disruption, in conjunction with interstrand cracks reflected by the solvent exposure of Trp-28 (orange) and Trp-114 (turquoise) (Fig. 5*B*), would give carboxypeptidase Y access to the centrally located β-strand h. With membrane-embedded TNF, the inaccessibility of Leu-157 to carboxypeptidase Y at both high and low pH is most likely due to resealing of cracked trimers or to failure of cracked trimers to insert rather than β-strand h displacement and insertion into the bilayer. Our rationale is that its ion pair Lys-11 (blue) and vicinal residues [Arg-6, Arg-32, and Arg-44 (all green); and Glu-23 (red)] are all surface accessible after TNF insertion (Fig. 5*A*). Moreover, crosslinking studies

(Fig. 3*A*) show that regardless of whether the target bilayer is fluid or frozen, membrane-inserted TNF exhibits a native-like trimeric structure. Hence, the structural alterations that we have detected in membrane-embedded TNF reflect changes within the confines of a trimer and not subunit dissociation.

Studies of the degree to which the physical state of the bilayer places constraints on protein binding and insertion can reveal important information on the types of interactions involved, which in turn can lead to new ways to alter target cell susceptibility. Use of frozen and fluid DMPC targets revealed that although TNF's vesicle binding and bilayer insertion activities both increase with decreasing pH, the two processes are not strictly identical. Results from several such studies show that TNF binds more efficiently to fluid vesicles than to frozen ones. With fluid vesicles at low pH, binding and insertion both saturate within 5–15 min. In contrast, binding to frozen targets saturates within 5–15 min but membrane insertion proceeds for up to 30 min. Despite lower binding, the insertion level noted at any given time was always greater with frozen membranes. Because studies with 12APS-GlcN have uncovered a wide variety of protein-specific insertion behaviors as a function of membrane physical state (33, 37–39), we are confident that results obtained with TNF reflect the behavior of the protein rather than the behavior of the probe.

Our model for TNF membrane penetration and channel formation (Fig. 6; see also ref. 24) is consistent with recent x-ray data on TNF-receptor cocrystals (36), with the notable disorder of the topmost loop regions of the TNF trimer (22, 23, 34, 35) and with the level of structural plasticity inherent in the nonsuperposability of the three monomers (22, 23, 34, 35). Indeed, Sprang and Eck (34) have speculated that this level of plasticity could account for the membrane-insertion activity of TNF, which like channel-forming activity (24) is low but detectable at pH 7 (Fig. 2*A*).

The fact that vesicle-inserted TNF retains its biological activity (R.L.B. and B.J.W., unpublished data) and voltage-gated channel activity (25–27), coupled with the notable increase in cytotoxicity observed when target cells are exposed to TNF at an acidic pH that disfavors receptor binding (18, 19), underscores the importance of TNF-membrane associations in the cytotoxic pathway of TNF. Since the only known intrinsic function of non-receptor-bound TNF is ion-channel activity (24–27), we propose that this activity may be responsible at least in part for the acid-enhanced effects of TNF on tumor cells (18, 19). Detailed knowledge of the formation, structure, and activity of the TNF channel, including modulatory conditions, should enable us to design experiments to test this prediction directly.

We thank Dr. Jeanne Perry for expert advice and support in the area of computer graphics and Christian Pettker and Steve Lessnick for technical assistance. This work was sponsored in part by National Institutes of Health (NIH) Grant GM22240 (to B.J.W.) and by American Cancer Society Grant IM-716 (to B.J.W.); R.L.B. was the recipient of NIH National Research Service Award 2 T32 HL07386.

1. Beutler, B. & Cerami, A. (1989) *Annu. Rev. Immunol.* **7,** 626–655.
2. Vassalli, P. (1992) *Annu. Rev. Immunol.* **10,** 411–452.
3. Tracy, K. J. & Cerami, A. (1993) *Annu. Rev. Cell Biol.* **9,** 317–343.
4. Loetscher, H., Pan, E. Y.-C., Lahm, H. W., Gentz, R., Brockhaus, M., Tabuchi, H. & Lesslauer, L. (1990) *Cell* **61,** 351–359.
5. Schall, T. J., Lewis, M., Koller, K. J., Lee, A., Rice, G. C., Wong, G. H., Gatanaga, T., Granger, G. A., Lentz, R., Raab, H., Kohr, W. J. & Goeddel, D. V. (1990) *Cell* **61,** 361–370.
6. Smith, C. A., Davis, T., Anderson, D., Solam, L., Beckmann, M. P., Jerzy, R., Dower, S. K., Cosman, D. & Goodwin, R. G. (1990) *Science* **248,** 1019–1023.
7. Kull, F. C., Jr., Jacobs, S. & Cuatrecasas, P. (1985) *Proc. Natl. Acad. Sci. USA* **82,** 5756–5760.
8. Nii, A., Fan, D. & Fidler, I. J. (1991) *J. Immunother.* **10,** 13–19.
9. Muchmore, A., Decker, J., Shaw, A. & Wingfield, P. (1990) *Cancer Res.* **50,** 6285–6290.
10. Lucas, R., Magez, S., De Leys, R., Fransen, L., Scheerlinck, J.-P., Rampelberg, M., Sablon, E. & De Baetselier, P. (1994) *Science* **263,** 814–817.
11. Smith, M. R., Munger, W. E., Kung, H.-F., Takacs, L. & Durum, S. K. (1990) *J. Immunol.* **144,** 162–169.
12. Morishige, H., Ohkuma, T. & Kaji, A. (1993) *Biochim. Biophys. Acta* **1151,** 59–68.
13. Tsujimoto, M., Yip, Y. K. & Vilcek, J. (1985) *Proc. Natl. Acad. Sci. USA* **82,** 7626–7630.
14. Kull, F. C., Jr., & Besterman, J. M. (1990) *J. Cell. Biochem.* **42,** 1–12.
15. Kull, F. C., Jr. & Cuatrecasas, P. (1981) *Cancer Res.* **41,** 4885–4890.
16. Niitsu, Y., Watanabe, N., Sone, H., Neda, H., Yamauchi, N. & Urushizaki, I. (1985) *Jpn. J. Cancer Res.* **76,** 1193–1197.
17. Liddil, J. D., Dorr, R. T. & Scuderi, P. (1989) *Cancer Res.* **49,** 2722–2728.
18. Baldwin, R. L., Chang, M. P., Bramhall, J., Graves, S., Bonavida, B. & Wisnieski, B. J. (1988) *J. Immunol.* **141,** 2352–2357.
19. Chang, M. P. & Wisnieski, B. J. (1990) *Infect. Immun.* **58,** 2644–2650.
20. Silver, I. A., Murrills, R. J. & Etherington, D. J. (1988) *Exp. Cell Res.* **175,** 266–276.
21. Mellman, I., Fuchs, R. & Helenius, A. (1986) *Annu. Rev. Biochem.* **55,** 663–700.
22. Jones, E. Y., Stuart, D. I. & Walker, N. P. C. (1989) *Nature (London)* **338,** 225–228.
23. Eck, M. J. & Sprang, S. R. (1989) *J. Biol. Chem.* **264,** 17595–17605.
24. Kagan, B. L., Baldwin, R. L., Munoz, D. & Wisnieski, B. J. (1992) *Science* **255,** 1427–1430.
25. Ernst, W. A., Mirzabekov, T., Kagan, B. L. & Wisnieski, B. J. (1994) *Biophys. J.* **66,** A204 (abstr.).
26. Kagan, B. L., Mirzabekov, T., Munoz, D., Baldwin, R. L. & Wisnieski, B. J. (1993) *Ann. N.Y. Acad. Sci.* **707,** 317–327.
27. Baldwin, R. L., Mirzabekov, T., Kagan, B. L. & Wisnieski, B. J. (1995) *J. Immunol.* **156,** 790–798.
28. Bychkova, V. E., Pain, R. H. & Ptitsyn, O. B. (1988) *FEBS Lett.* **238,** 231–234.
29. Zalman, L. S. & Wisnieski, B. J. (1985) *Infect. Immun.* **50,** 630–635.
30. Chamberlain, J. P. (1979) *Anal. Biochem.* **98,** 132–135.
31. Matsudaira, P. (1987) *J. Biol. Chem.* **262,** 10035–10038.
32. Farahbakhsh, Z. T., Baldwin, R. L. & Wisnieski, B. J. (1987) *J. Biol. Chem.* **262,** 2256–2261.
33. Wisnieski, B. J. & Bramhall, J. S. (1981) *Nature (London)* **289,** 319–321.
34. Sprang, S. R. & Eck, M. J. (1992) in *Tumor Necrosis Factors: The Molecules and Their Emerging Role In Medicine*, ed. Beutler, B. (Raven, New York), pp. 11–32.
35. Sprang, S. R. & Eck, M. J. (1990) in *Current Research in Protein Chemistry: Techniques, Structure, and Function*, ed. Villafranca, J. J. (Academic, New York), pp. 383–394.
36. Banner, D. W., D'Arcy, A., Janes, W., Gentz, R., Schoenfeld, H.-J., Broger, C., Loetscher, H. & Lesslauer, W. (1993) *Cell* **73,** 431–445.
37. Hu, V. W., Esser, A. F., Podack, E. R. & Wisnieski, B. J. (1981) *J. Immunol.* **27,** 380–386.
38. Ishida, B., Cawley, D. B., Reue, K. & Wisnieski, B. J. (1983) *J. Biol. Chem.* **258,** 5933–5937.
39. Zalman, L. S. & Wisnieski, B. J. (1984) *Proc. Natl. Acad. Sci. USA* **81,** 3341–3345.